# COMPUTATIONAL OPTICAL SECTIONING MICROSCOPY USING AN ENGINEERED PSF WITH REDUCED DEPTH VARIABILITY -- PROOF OF CONCEPT

*Shuai Yuan and Chrysanthe Preza*

Department of Electrical and Computer Engineering, the University of Memphis, Memphis

## ABSTRACT

In this simulation study, an engineered point-spread function (PSF) with reduced depth variability (due to depth-induced aberrations) was applied to three-dimensional computational optical-sectioning microscopy (COSM) imaging to investigate its impact on image restoration. Intermediate synthetic images from PSF-engineered COSM in the presence of aberrations were computed and then processed using a depth-variant expectation maximization algorithm. The restored images were compared to images simulated for traditional COSM. Results show that PSF-engineered COSM achieves better image restoration than conventional COSM and has the potential to improve imaging in the presence of depth-induced aberrations.

***Index Terms***— Wave front encoding, Computational Optical Sectioning Microscopy, Expectation Maximization, cubic phase modulation

## 1. INTRODUCTION

Computational imaging plays an important role in the advances achieved in three-dimensional (3-D) fluorescence microscopy [1]. A major challenge in 3-D microscopy applied to most biomedical applications, is the inherent depth variability in the imaging process, i.e., as the imaging depth increases within a 3-D sample the 3-D point spread function (PSF) changes [2, 3]. As it is known, this is due to the refractive index (RI) mismatch in the imaging layers [4].

The widespread use of computational optical sectioning microscopy (COSM) [5] for 3-D imaging has motivated the development of new computational methodologies to improve the restored image quality by accounting for this depth variability while reducing computational complexity [6-9]. In traditional COSM, only a single 3-D PSF is used in the image reconstruction process [10], but when the 3-D PSF depth variability is significant, the use of multiple depth-variant (DV) PSFs is necessary to reduce undesirable computation artifacts [6]. Computational complexity generally increases with the number of 3D DV-PSFs used in the computations [11] and thus, reducing the sensitivity of the 3D PSF to the depth-induced aberrations, such as spherical aberration (SA), could decrease the number of PSFs needed to achieve the desired image quality.

One promising approach for reducing the depth variability of the 3-D PSF is via PSF engineering [12, 13] achieved by placing a phase mask at the pupil plane of the imaging lens to encode the wavefront emerging from an imaging system. PSF engineering via wavefront encoding has been implemented successfully to enhance optical system properties [14, 15]. For example, in extended depth-of-field (EDOF) microscopy, a wavefront encoded (WFE) PSF, engineered to be insensitivity to defocus, produces an intermediate image which is then digitally processed to decode the information in a 3-D object [16]. In each 2-D processed image, all structures distributed in the 3-D object are visible well-focused as the microscope is focused at different depths of the object (regardless of the location of the structures in the 3D volume).

In a recent study, we investigated the use of WFE with different cubic-phase mask designs as an approach to improve COSM performance in the presence of SA [13]. The sensitivity of various engineered WFE-PSFs to defocus and SA was quantified through the use of mean-square-error (MSE) based merit functions computed between the layers of single WFE-PSF and also between two 3D DV WFE-PSFs. Results from this study guided the selection of a WFE-PSF based on a generalized cubic phase mask (GCPM) design that has low sensitivity to SA and high sensitivity to defocus suitable for COSM.

The selected WFE-PSF for COSM was also shown to have a greater extend both laterally and axially when compared to the conventional COSM PSF. An important question is the utility of the WFE-PSF in image restoration using algorithms developed for traditional COSM. In this paper, we present restored images of a test object that investigate the feasibility of WFE-COSM imaging via a simulation study.

The paper is organized as follows. Section 2 reviews image formation theory for a WFE widefield microscope in the presence of SA as well as methods used in the simulations for the computation of synthetic and restored images in this study. Restored images of a test object, computed using a depth-variant image estimation method applied to WFE images, are presented and compared to images from traditional COSM imaging in Section 3. Results are further discussed in Section 4.

## 2. THEORY AND METHODS

### 2.1. Image formation model

In a WFE microscope system a phase mask with phase $\phi(f_x, f_y)$ is inserted at the back focal plane of the imaging lens. The phase mask modifies the phase of the generalized pupil function and thereby changes the properties of the system's PSF. The WFE-system can be characterized by a PSF that varies with both the depth $z = z_i$ at which the microscope is focused and the location of the point light source, $z = z_o$, along the optical axis:

$$h_{z_i,z_o}(x,y) = \left| \mathrm{F}^{-1}\left\{ H(f_x,f_y) e^{j(2\pi/\lambda)W(f_x,f_y;z_i,z_o)} e^{j\phi(f_x,f_y)} \right\} \right|^2, \quad (1)$$

where $H(f_x, f_y)$ is the clear circular aperture (CCA) pupil function, $\lambda$ is the emission wavelength, $W(f_x, f_y; z_i, z_o)$ is the optical-path-length error due to defocus and SA as a function of the normalized spatial frequencies $f_x$ and $f_y$, and $F^{-1}\{\bullet\}$ denotes a 2-D inverse Fourier transform. The phase of the selected GCPM design is given by [13]:

$$\phi(f_x,f_y) = 50\left(f_x^3 + f_y^3\right) - 50\left(f_x^2 f_y + f_x f_y^2\right).$$

The intensity in the image formed by a WFE-system characterized by a 3D PSF (Eq. 1) can be modeled by the superposition integral:

$$g(\mathbf{x}_i) = \iiint_O h_{WFE}(x_i - x_o, y_i - y_0, z_i, z_o) s(\mathbf{x}_o) d\mathbf{x}_o, \quad (2)$$

where $\mathbf{x}_i = (x_i, y_i, z_i)$ is a point in the image space, $\mathbf{x}_o = (x_o, y_o, z_o)$ is a point in the object space $O$, $s(\mathbf{x}_o)$ is the intensity of the underlying object and

$$h_{WFE}(x,y,z_i,z_o) = h_{z_i,z_o}(x,y).$$

Eq. (2) has been approximated by a strata-based model that uses only a finite number of 3D DV PSFs in the computation of the image formation model [6].

### 2.2. Synthetic images

Simulated intermediate images from WFE-COSM (Fig. 1c) and from conventional COSM were computed using the strata-based approach with 2 strata and a computer-generated test object that consists of 3 small spheres (1 μm in diameter) centered at different depths (Fig. 1b): 1, 5, and 9 μm on a 512 x 512 x 300 grid with voxels of size 0.1 x 0.1 x 0.1 μm$^3$. The ($x_o$, $y_o$) coordinates of the three spheres are: (5 μm, 5 μm), (0 μm, 0 μm), and (-5 μm, -5 μm), from top to bottom correspondingly, with the origin of the $x_o y_o$ plane taken at the center of the grid. The origin along the $z_o$ axis is placed at the 100$^{th}$ plane of the volume.

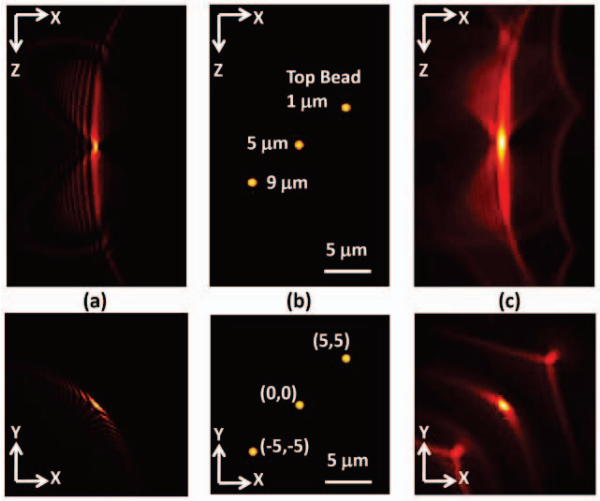



**Fig. 1.** Synthetic intermediate images from WFE-COSM. XZ (top) and XY (bottom) images: (a) of the center-cut view of the 3-D GCPM-WFE PSF computed at depth $z_o$ = 0 μm; (b) of the 3-bead object projection views along Y and Z, respectively; (c) of the center-cut view of the simulated image.

In order to compute the synthetic images, 3D DV complex-amplitude PSFs for conventional widefield microscopy were computed using the Gibson and Lanni PSF model [2] which is readily available to us via the PSF computation module of our COSM Open Source (COSMOS) software package [17]. DV PSFs for depths $z_o$ = 0, 5, and 10 μm were computed. PSFs at other depths needed in the computation, are approximated by the strata approach by linear interpolation of two PSFs at the boundaries of a stratum [6]. The DV PSFs were computed on a 512 x 512 x 300 grid with voxels of size 0.1 x 0.1 x 0.1 μm$^3$ for a 60x/1.2 NA oil-immersion objective lens (RI = 1.515) using emission wavelength $\lambda$ = 633 nm and assuming that the light point source is located at a different depth ($z_o$ = 0, 5 and 10μm) in water (RI = 1.33) below the coverslip.

The DV WFE-PSFs (Fig. 1a) were calculated from Eq. (1) implemented in Matlab, using the 2D Fourier transform of the conventional complex-amplitude PSFs. The phase of the GCPM was computed within a circular pupil aperture (on a 194 x 194 grid with $f_x$ and $f_y$ ranging from [-1 1] over the 194 columns/rows) and then padded to a 512 x 512 grid so that the circular aperture in the pattern matches the circular pupil aperture of the objective lens.

### 2.3. Image restoration

The depth-variant expectation maximization (DVEM) algorithm [6] was used to process COSM images from both the WFE and the traditional system for comparison, using

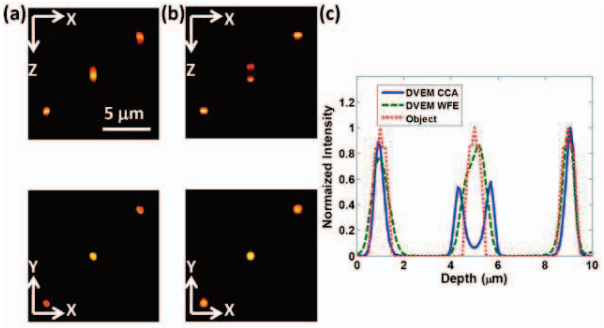



**Fig. 2.** Comparison of reconstructed images of the 3-bead object: (a) from WFE-COSM and (b) from CCA-COSM. Images shown are projections views along-Y (top) and along-Z (bottom) computed from the reconstructions. (c) Along-XY projection intensity profile of reconstructed images and the object vs. depth below the coverslip.

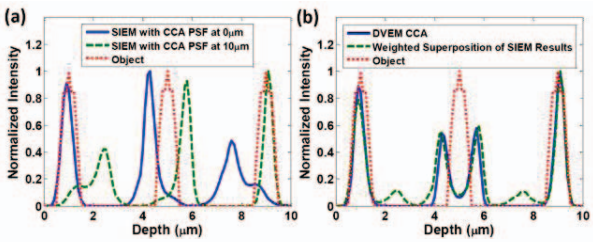



**Fig. 3.** Comparison of SIEM and DVEM reconstruction results obtained from the same conventional COSM image using different sets of CCA-PSFs. (a) Along-XY projection intensity profiles from reconstructed images using SIEM and a single PSF (computed at depths $z_o = 0$ μm and $z_o = 10$ μm ) vs. z depth, compared to a similar projection profile computed from the object; (b) Along-XY projection intensity profiles from reconstructed images and the object vs. depth below the coverslip.

only one stratum with its boundary DV-PSFs defined at depths $z_o = 0$ μm and 10 μm below the coverslip.

Synthetic images from the conventional system were also processed with the space-invariant expectation maximization (SIEM) algorithm [18] (which uses only a single PSF for the processing), in order to verify results obtained from the DVEM algorithm applied to these images. For both algorithms, results were examined at different number of iterations. The SIEM and DVEM methods used for image restoration in this study are implemented in the COSMOS estimation module [17].

## 3. RESULTS

XY and XZ cut views of the WFE-COSM simulated image (Fig. 1c) of the three-bead test object (Fig. 1b) have a distorted appearance due to the WFE-PSF (Fig. 1a). As evident from Fig. 1(a), the WFE-PSF has a larger extend in both the XY and XZ plane than the conventional PSF (images not shown). Due to the extension of WFE PSFs along the Z axis, contributions from the top and bottom beads are clearly seen in the center-cut view of the intermediate image (Fig. 1 (c), bottom) although only one bead is present in the center Z plane. Projection views of the object along-Y (Fig. 1 (b), top) and along-Z (Fig. 1(b), bottom) were computed to facilitate visualization of the 3 beads in single 2-D images.

Results obtained from processing the simulated intermediate images using the DVEM algorithm with one stratum (i.e., two DV PSFs as discussed in Section 2.3) are summarized in Fig. 2. The reconstructed images from WFE-COSM and conventional COSM (also referred to as the clear circle aperture (CCA) COSM) are shown in Fig. 2 (a) and Fig. 2 (b), respectively. The intensity *z*-profiles after a 2-D XY-plane projection of the reconstructed 3-D images shown in Fig. 2(a) and Fig. 2(b) are plotted vs. the depth along the Z axis in Fig. 2(c). After the 2-D XY projection the resulting z-profile was normalized to have a peak value equal to 1.

In both cases, the beads located at the top (i.e., at 0 μm) and at the bottom (i.e., at 10 μm) were reconstructed very well as quantified by the profiles in Fig. 2(c). However, a significant artifact is evident in the reconstructed image from the conventional CCA-COSM system: the center bead was reconstructed into two small beads (Fig. 2b). This artifact is not present in the reconstructed image obtained from the WFE-COSM system. In this case, the restored center bead is slightly elongated along the Z axis (Fig 2a).

## 4. DISCUSSION

The artifact observed in the reconstruction of the center bead from the conventional COSM images (Fig. 2b), was further investigated and it was confirmed to be due to the CCA-PSF depth variability. This was accomplished by processing the conventional image using the SIEM and a single CCA-PSF computed at two different depths: $z_o = 0$ μm and $z_o = 10$ μm. The results obtained in both cases are summarized in Fig 3(a) and show that, although the three object beads are reconstructed, their positions at *z*-depths other than the depth where the PSF was computed are shifted in the direction toward the PSF depth. Because of this shift and its direction, the reconstructed position of the center bead ( $z_o = 5$ μm ) in each of the two cases is off the center position in opposite directions. A weighted superposition of the two *z*-profiles from the two SIEM results is also shown in Fig. 3(a). The weight was linearly determined by the relative distance from the two depths to simulate what DVEM computes [6]. The profile of the center bead from the superposition is very close to the profile from the one-stratum DVEM result computed from the conventional COSM image and two CCA-PSFs at depths $z_o = 0$ μm and $z_o = 10$ μm.

The comparison in Fig. 2 shows that using WFE in COSM to reduce PSF variability as presented in Ref [13] can improve the performance of COSM in the presence of SA. Our image reconstruction results obtained from the WFE-COSM images of the 3-bead object show a reasonable agreement with the original object demonstrating a proof of concept that WFE-PSFs can be used with the DVEM algorithm developed for traditional COSM to process images from a WFE microscope.

## 5. CONCLUSION

In this paper, results from a proof-of-concept simulation were presented to illustrate the benefit of integrating PSF engineering with a depth-variant estimation approach for COSM. Our results showed that using WFE in COSM to reduce PSF depth-variability yields better image restoration and thereby improving the performance of COSM imaging in the presence of depth-induced SA.

## 6. ACKNOWLEDGEMENTS

This work was supported by the National Science Foundation (CAREER award DBI-0844682 and IDBR award DBI-0852847, PI: C. Preza) and the University of Memphis.

## 7. REFERENCES

[1] P. M. Carlton, J. Boulanger, C. Kervrann, J.-B. Sibarita, J. Salamero, S. Gordon-Messer, D. Bressan, J. E. Haber, S. Haase, L. Shao, L. Winoto, A. Matsuda, P. Kner, S. Uzawa, M. Gustafsson, Z. Kam, D. A. Agard, and J. W. Sedat, "Fast live simultaneous multiwavelength four-dimensional optical microscopy," *Proceedings of the National Academy of Sciences,* vol. 107, pp. 16016-16022, 2010.

[2] S. F. Gibson and F. Lanni, "Experimental Test of an Analytical Model of Aberration in an Oil-Immersion Objective Lens Used in 3-Dimensional Light-Microscopy," *Journal of the Optical Society of America a-Optics Image Science and Vision,* vol. 9, pp. 154-166, Jan 1992.

[3] P. Török, P. Varga, and G. Nemeth, "Analytical solution of the diffection integrals and interpretation of wave-front distortion when light is focused through a planar interface between materials of mismatched refractive indices," *Journal of the Optical Society of America A-Optics Image Science and Vision,* vol. 12, pp. 2660-2671, 1995.

[4] S. F. Gibson and F. Lanni, "Experimental test of an analytical model of aberration in an oil-immersion objective lens used in three-dimensional light microscopy," *Journal of the Optical Society of America A-Optics Image Science and Vision,* vol. 9, pp. 54–66, 1992.

[5] D. A. Agard, "Optical sectioning microscopy: Cellular Architecture in Three Dimensions," *Annual Review of Biophysics and Bioengineering,* vol. 13, pp. 191–219, 1984.

[6] C. Preza and J. A. Conchello, "Depth-variant maximum-likelihood restoration for three-dimensional fluorescence microscopy," *Journal of the Optical Society of America a-Optics Image Science and Vision,* vol. 21, pp. 1593-1601, Sep 2004.

[7] Z. Kam, P. Kner, D. A. Agard, and J. W. Sedat, "Modelling the application of adaptive optics to wide-field microscope live imaging," *Journal of Microscopy-Oxford,* vol. 226, pp. 33-42, 2007.

[8] S. Yuan and C. Preza, "3D fluorescence microscopy imaging accounting for depth-varying point-spread functions predicted by a strata interpolation method and a principal component analysis method," in *Three-Dimensional and Multidimensional Microscopy: Image Acquisition and Processing XVIII*, San Franscisco, 2011, p. 79040M.

[9] J. W. Shaevitz and D. A. Fletcher, "Enhanced three-dimensional deconvolution microscopy using a measured depth-varying point-spread function," *Journal of the Optical Society of America A-Optics Image Science and Vision,* vol. 24, pp. 2622-2627, 2007.

[10] J.-B. Sibarita, "Deconvolution Microscopy," in *Microscopy Techniques*. vol. 95, J. Rietdorf, Ed., ed: Springer Berlin / Heidelberg, 2005, pp. 1288-1291.

[11] C. Preza and V. Myneni, "Quantitative depth-variant imaging for fluorescence microscopy using the COSMOS software package," in *Three-Dimensional and Multidimensional Microscopy: Image Acquisition and Processing Xvii*, 2010, p. 757003.

[12] G. Saavedra, I. Escobar, R. Martinez-Cuenca, E. Sanchez-Ortiga, and M. Martinez-Corral, "Reduction of spherical-aberration impact in microscopy by wavefront coding," *Optics Express,* vol. 17, pp. 13810-13818, Aug 3 2009.

[13] S. Yuan and C. Preza, "Point-spread function engineering to reduce the impact of spherical aberration on 3D computational fluorescence microscopy imaging," *Optics Express,* vol. 19, pp. 23298-23314, 2011.

[14] E. R. Dowski and W. T. Cathey, "Extended depth of field through wave-front coding," *Applied Optics,* vol. 34, pp. 1859-1866, 1995.

[15] S. R. P. Pavani and R. Piestun, "Three dimensional tracking of fluorescent microparticles using a photon-limited double-helix response system," *Optics Express* vol. 16, pp. 22048-22057, 2008.

[16] S. C. Tucker, W. T. Cathey, and J. Edward R. Dowski, "Extended depth of field and aberration control for inexpensive digital microscope systems," *Optics Express,* vol. 4, pp. 467-474, 1999.

[17] http://cirl.memphis.edu/COSMOS.

[18] J.-A. Conchello, "Super-resolution and convergence properties of the expectation-maximization algorithm for maximum-likelihood deconvolution of incoherent images," *Journal of the Optical Society of America A-Optics Image Science and Vision,* vol. 15, pp. 2609-2620, 1998.